JOC The Journal of Organic Chemistry

Article

pubs.acs.org/joc

Substitution-Assisted Stereochemical Control of Bispidone-Based Ligands

Tarik Legdali,[†] Amandine Roux,[†] Carlos Platas-Iglesias,[‡] Franck Camerel,[§] Aline M. Nonat,*[,†] and Loïc J. Charbonnière*[,†]

[†]Laboratoire d'Ingénierie Moléculaire Appliquée à l'Analyse, IPHC, UMR 7178 CNRS/UdS, ECPM, Bât R1N0, 25 rue Becquerel, 67087 Strasbourg Cedex 02, France

[‡]Departamento de Química Fundamental, Universidade da Coruña, Campus da Zapateira- Rúa da Fraga 10, 15008, A Coruña, Spain

[§]Laboratoire Matière Condensée et Systèmes Électroactifs, Institut des Sciences Chimiques de Rennes, UMR 6226, 263 Avenue du General Leclerc, CS 74205, 35042 Rennes Cedex, France

Supporting Information

ABSTRACT: Three new bispidone derivatives substituted by methylenecarboxylic ethyl ester groups have been synthesized in high yields as potential ligands for ^{64}Cu complexation and PET imaging. Their solution and solid-state structures have been determined by ^{1}H NMR spectroscopy and X-ray crystallography. These studies reveal a strong rigidity of the bicycle, which adopts either a chair−chair or a boat−chair conformation depending on the substituents in the N3 and N7 positions. A methyl substituent at N3 stabilizes the chair−chair conformation, whereas ethylacetate or 2-pyridylmethyl groups induce a considerable stabilization of the boat−chair conformation. However, when introduced in the position N7, a 2-pyridylmethyl substituent stabilizes the chair−chair isomer. The relative energies of the isomers and the isomerization process have been modeled by density functional theory calculations on a series of six N-substituted bispidones, including those newly synthesized. The subtle influence of the substituents has been related not only to the effect of steric hindrance on the thermodynamic stability but also to the presence of weak H-bonding interactions involving hydrogen-bonding acceptors, such as pyridylmethyl or ethylacetate substituents, and donors, such as C(sp2)-H of the pyridyl rings or C(sp3)-H at various positions of the bispidone skeleton.

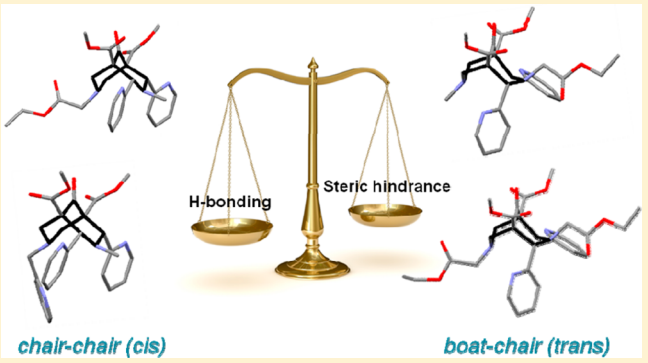

INTRODUCTION

Since their first discovery by Petreko-Krischenko in 1942,[1] 3,7-diazabicyclo[3.3.1]nonanes, also called bispidines (Scheme 1), have attracted considerable interest as opioid-like analgesic drugs[2,3] or as highly potent bradycardic agents with antiarrhythmic properties.[4,5] In particular, the strong rigidity of the bispidine skeleton allows a fine control of the ligand−receptor affinity. Previous studies have demonstrated that variation on the substituents attached to the nitrogens in positions 3 and 7 could result in a complete loss of affinity.[6] This strong influence of the substitution was explained by variations of the stereochemistry of the bicyclic ring. Indeed, the bispidine skeleton usually adopts one of the three following conformations: chair−chair (cc), chair−boat (cb), or boat−chair (bc) (Scheme 1). The boat−boat (bb) conformation was found to be energetically unfavorable.[7] Moreover, in the case of 2,4-substituted bispidines, the substituents in positions 2 and 4 can be found in axial or equatorial positions, leading to three possible diastereoisomers per conformation (Scheme 1). Derivatives in the cc conformation were found to display the best affinity for opioid[8] and 5-HT3 receptors.[9]

Moreover, the strong rigidity and preorganization of the cc conformers have promoted the use of 2,4-substituted bispidines for the synthesis of complexes with transition-metal ions,[10,11] such as $V^{4/5+}$,[12] Fe^{2+},[13,14] $Co^{2+/3+}$,[15] Cu^{2+},[16] and Ru^{2+}.[17] Attention has been focused on their applications as models for a variety of metalloenzymes and in catalysis as well as, more recently, bifunctional chelates for Cu^{2+} radioisotopes for positron emission tomography (PET).[18] Indeed, radiolabeled $^{64}Cu^{2+}$ complexes display a long half-life (^{64}Cu, $t_{1/2}$ = 12.7 h, β^+, 17.8%, 653 K eV),[19] which offers a great potential for the monitoring of biological cell function and molecular processes in vivo.[20−23]

Preliminary studies of 2,4-pyridyl-substituted bispidine ligands have demonstrated the formation of Cu^{2+} complexes with high kinetic and thermodynamic stabilities, fast kinetics of complexation, and a particularly good selectivity for Cu^{2+}.[11] We can foresee that the introduction of well-adapted coordinating groups at N3, N7, C2, and C4 should allow for tuning the

Received: October 19, 2012
Published: November 26, 2012

Scheme 1. 2,4-Substituted 3,7-Diazabicyclo[3.3.1]nonanes (Bispidines): General Structure (Left) and Representation of the Energetically Favored Conformations of the Bicycle (cc, cb, and bc) as Well as the Configuration of the 2,4 Substituents (*Cis* and *Trans*)

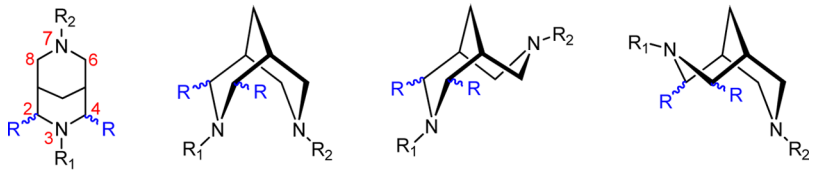

ligand affinity and selectivity for Cu^{2+}, providing a favorable cc conformation together with a *cis* arrangement of the substituents in positions 2 and 4. So far, mostly 2,4-pyridyl-substituted bispidines with 2-pyridylmethyl or 2-(2-pyridyl)-ethyl substituents at N3 and N7 have been synthesized, and the diastereoisomers of interest, in which the substituents at C2 and C4 are in the equatorial position, have been isolated in yields varying from 25% to 68%.[13] In the current study, we report the synthesis of three novel bispidones with methyl-enecarboxylic ethyl ester pendant arms (L_2–L_4, Scheme 2).

Scheme 2. Tetradentate (L_0), Pentadentate (L_1, L_2, L_3), and Hexadentate (L_4, L_5) Bispidone Ligands and Their Atom Numbering for Crystallographic and NMR Studies

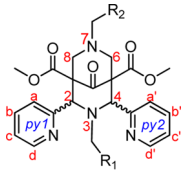

L_0 : $R_1 = R_2 = H$
L_1 : $R_1 = H$, $R_2 = py$
L_2 : $R_1 = H$, $R_2 = COOEt$
L_3 : $R_1 = COOEt$, $R_2 = H$
L_4 : $R_1 = R_2 = COOEt$
L_5 : $R_1 = R_2 = py$

Their solution and solid-state structures have been investigated by ^1H NMR spectroscopy, X-ray diffraction, and DFT calculations in order to gain a better understanding of the factors that control their stereochemistry upon substitution, as well as of the mechanism responsible for the *cis* ↔ *trans* isomerization process. For a better comprehension of the stereochemistry of these newly synthesized bispidones, model compounds with 2-pyridylmethyl substituents (L_1 and L_5, Scheme 2) were also investigated.

RESULTS AND DISCUSSION

Synthesis. The synthesis of bispidones L_1–L_4 (bispidone = 9-oxo-3,7-diazabicyclo[3.3.1]nonane) was achieved in two steps by using two consecutive double-Mannich reactions. Piperidone intermediates, P_1 and P_2, were first synthesized from commercially available dimethyl-1,3-acetonedicarboxylate, 2-pyridinecarboxaldehyde, and a primary amine R_1-NH_2, allowing for the introduction of the R_1 substituent (R_1 = Me, CH_2COOEt). In the second step, these piperidones were reacted with formaldehyde and a second amine R_2-NH_2 (R_2 = Me, CH_2COOEt, CH_2py) (Scheme 3).

Depending on the relative position of the pyridyl groups with respect to the central six-membered ring, the piperidone intermediates can exist as *cis* or *trans* isomers (Scheme 4).

Scheme 4. Possible Isomers of the Piperidone Intermediates

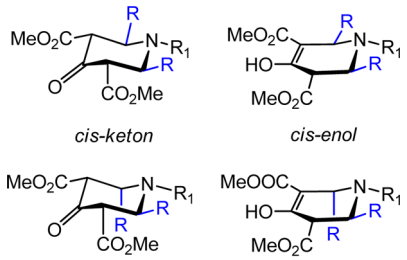

Additionally, keto–enol equilibrium is also possible for both the *cis* and the *anti* forms so that four isomers (*cis*-enol, *cis*-keto, *trans*-keto, and *trans*-enol) can be present in solution depending on the conditions and on the nature of the substituent R_1 (Scheme 4).[24] P_1 has been isolated in 70% yield as a mixture of three isomers (*cis*-enol, *cis*-keto, and *trans*-enol), as observed by ^1H NMR in CD_3OD. In contrast, P_2 was isolated in 62% yield as the pure *trans*-enol isomer, as evidenced from its ^1H NMR spectrum.

In line with previous publications,[24] the configuration of the piperidone intermediate does not seem to have any influence on the final configuration of the bispidone ligand. In the case of ligands L_1 and L_2, a mixture of isomers in different configurations (*cis* and *trans*) was first formed and the pure

Scheme 3. Synthesis of the Bispidone Ligands L_1–L_4

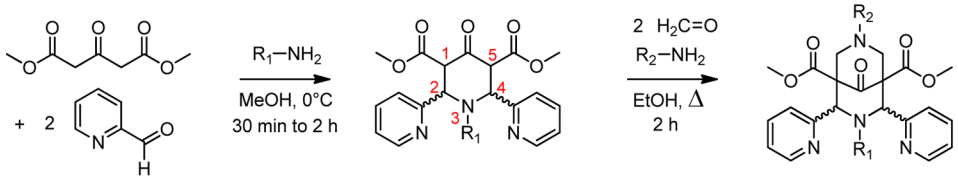

P_1 : R_1 = Me
P_2 : R_1 = CH_2COOEt

L_1 : R_1 = Me, R_2 = CH_2py
L_2 : R_1 = Me, R_2 = CH_2COOEt
L_3 : R_1 = CH_2COOEt, R_2 = Me
L_4 : R_1 = CH_2COOEt, R_2 = CH_2COOEt

dx.doi.org/10.1021/jo302248c | J. Org. Chem. 2012, 77, 11167–11176

Table 1. Crystallographic Data for Ligands L_1, L_2, and L_4

	L_1	L_2	L_4
formula	$C_{28}H_{29}N_5O_5$	$C_{26}H_{30}N_4O_7$	$C_{29}H_{34}N_4O_9$
molecular wt ($g\cdot mol^{-1}$)	515.56	510.54	582.60
temp (K)	150(2)	173(2)	173(2)
cryst size (mm)	0.42 × 0.28 × 0.11	0.30 × 0.25 × 0.20	0.40 × 0.5 × 0.30
cryst system	monoclinic	monoclinic	orthorhombic
space group	$P2_1/n$	$P2_1/c$	$Fdd2$
unit cell dimen. (Å, deg)	a = 10.5690(5)	a = 14.8091(4)	a = 36.2985(6)
	b = 21.4775(14)	b = 11.8613(4)	b = 34.2014(8)
	c = 11.5781(7)	c = 14.8551(4)	c = 9.2314(2)
	β = 98.834(2)	β = 100.775(2)	
volume ($Å^3$); Z	2597.0(3); 4	2563.37(13); 4	11460.4(4); 16
density (calcd) ($g\cdot cm^{-3}$)	1.319	1.323	1.351
abs. coeff. (mm^{-1})	0.093	0.097	0.101
$F(000)$	1088	1080	4928
θ_{max}	27.47	27.46	27.48
reflns collected	23421	25582	21205
independent reflns	5924	5860	5905
$I > 2\sigma(I)$ reflns	4401	4496	5407
params	334	338	383
R1, wR2 ($I > 2\sigma(I)$)	0.041, 0.093	0.0566, 0.1418	0.0435, 0.1086
R1, wR2 (all data)	0.0604, 0.1095	0.0832, 0.1555	0.0490, 0.1164
largest diff. peak, hole (e $Å^{-3}$)	0.287, −0.201	0.359, −0.389	0.204, −0.263

cis isomers were obtained as white powders in 55% and 62% yield, respectively, upon recrystallization from boiling EtOH. Ligand L_1 had previously been isolated in the *cis* configuration by Börzel et al,[13] although in a twice lower yield (25%). A significant improvement of the reaction yield was achieved by carrying out a "one-pot" reaction in EtOH, without isolating intermediate P_1. The syntheses of ligand L_3 and L_4 gave rise to single species, which were isolated as white solids in 86% and 90% yields, respectively, after recrystallization. The lack of symmetry observed in the NMR spectra of these ligands point to the formation of *trans* isomers. The determination of the solution structures of ligands L_1–L_4, as well as the solid-state structures of L_1, L_2, and L_4, is detailed below.

Structural Studies of L_1, L_2, and L_4 in the Solid State. As mentioned in the Introduction, the fused six-membered rings of substituted 3,7-diazabicyclo[3.3.1]nonan-9-one usually adopt one of the three energetically favored conformations, chair–chair (cc), chair–boat (cb), or boat–chair (bc) (Scheme 1), whereas the boat–boat conformation was found to be very energetically unfavorable. Each conformation can give rise to three diastereoisomers depending on the position of the aryl substituents at C2 and C4 relative to the bicyclic skeleton (axial or equatorial positions), among which the *cis* (2*S*,4*R* or 2*R*,4*S*) and *trans* (2*S*,4*S* or 2*R*,4*R*) configurational isomers are the most stable (Scheme 2).[1] The *cis* configuration, with the two substituents at C2 and C4 being in the equatorial positions, is usually found for cc or cb isomers. So far, the cb conformation has only been observed in bispidones with bulky substituents in the R_2 position or in doubly protonated diazabicycles.[1,7,14] The bc conformation, with a boat in the higher-substituted piperidone ring, has long been considered very unlikely to occur because it was postulated to occur through epimerization of the carbon atoms bearing the aryl substituents.[1] To the best of our knowledge, only the N3-ethyl, N3-propyl, N3-butyl, and N3-allyl bispidones were isolated in such a conformation and with a *trans* configuration of the pyridyl substituents at C2 and C4.[25] To get a better understanding of the influence of the substitution on the stereochemistry of the ligands, the structures of L_1, L_2, and L_4 have been elucidated by X-ray diffraction.

Single crystals of ligands L_1, L_2, and L_4 were obtained by slow evaporation of ethanol or methanol solutions. The corresponding molecular structures are depicted in Figures 1, 2, and 3. Crystallographic data as well as selected geometrical data are summarized in Tables 1 and 2, respectively. As expected, all

Table 2. Selected Experimental Structural Data of L_1, L_2, L_4, and $[Cu(L_1')Cl]^+$ (Distances in Å, Angles in deg)

	L_1	L_2	L_4	$[Cu(L_1')Cl]^+$
	distances (Å)			
N3···N7	2.935(2)	2.888(2)	3.473(2)	2.915
$N_{py1}\cdots N_{py2}$	7.241(2)	7.186(2)	6.639(2)	3.995
	twist angles between pyridine rings (deg)			
py1···py2	15.4	20.2	62.9	23.5

C=O bond lengths are consistent with double bonds (1.210(2) Å for L_1, 1.205(2) Å for L_2, and 1.201(2) Å for L_4) since the second cyclization step prevents tautomerization to the enol form.

Ligands L_1 and L_2 crystallize in the monoclinic space groups $P2_1/n$ and $P2_1/c$, respectively. The two bispidone bicyclic rings display a chair–chair conformation with the pyridyl rings in a *cis*-symmetrical configuration (Figures 1 and 2). The pyridine fragments py1 and py2 are almost coplanar, their least-squares planes intersecting at 15.44° for L_1 and 20.18° for L_2. As previously reported for other bispidone derivatives,[26] the chair–chair conformation brings the bicyclic nitrogen atoms in close proximity, leading to a highly preorganized skeleton favorable for metal complexation. As a comparison, the N3···N7 distance in L_1 and L_2 is of the same order of magnitude than the N3···N7 distance measured in the Cu(II) complex $[Cu(L_1')Cl]^+$, where L_1' is the analogue of L_1 in which the central ketone is in its hydrated form (Table 2).[27] The main

dx.doi.org/10.1021/jo302248c | J. Org. Chem. 2012, 77, 11167–11176

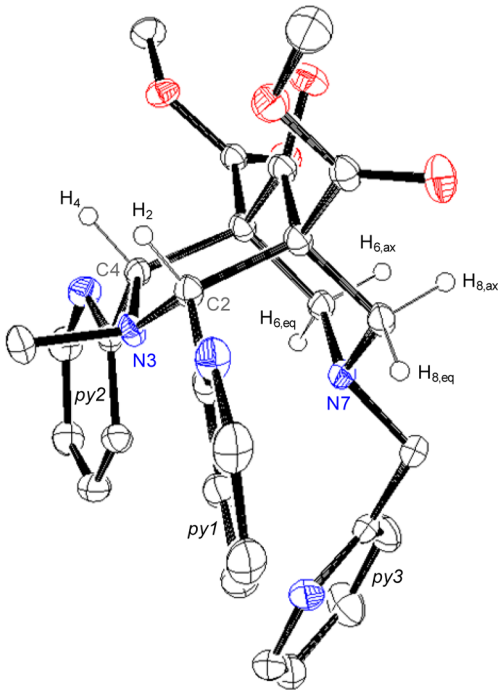

Figure 1. ORTEP drawing of ligand L_1 with the main numbering scheme. Thermal ellipsoids are drawn at the 30% probability level. H atoms are partially omitted for the sake of clarity.

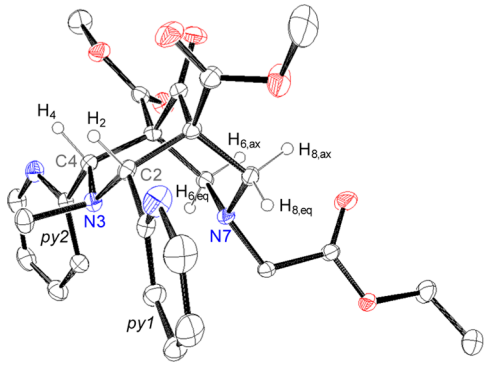

Figure 2. ORTEP drawing of ligand L_2 with the main numbering scheme. Thermal ellipsoids are drawn at the 30% probability level. H atoms are partially omitted for the sake of clarity.

reorganization that occurs upon metal complexation consists of the rotation of the pyridine donors py1 and py2 around the C–C bond linking them to the bispidone skeleton. In ligands L_1 and L_2, such as in other already described bispidine derivatives, the pyridines py1 and py2 are rotated away from the coordination site by approximately 180° to minimize the repulsion between the lone pairs of the nitrogen atoms of py1, py2, and N3.[10,28] Moreover, in ligand L_1, the pyridyl substituent at N7 is stabilized by a hydrogen-bonding interaction between its nitrogen atom and the proton H_a of the pyridyl group anchored at C2 (d_{H_a-N} = 2.818(2) Å, d_{C_a-N} = 3.643(2) Å, NH_aC_a = 145.80(9)°).

Interestingly, the bispidone skeleton of L_4 adopts a boat–chair (bc) conformation (Figure 3). Thus, L_4 represents, together with the N3-ethyl, N3-propyl, N3-butyl, and N3-allyl derivatives,[25] one of the few bispidone derivatives being isolated in such a conformation. For instance, ligand L_5, which contains two methylpyridyl substituents in positions N3 and N7,

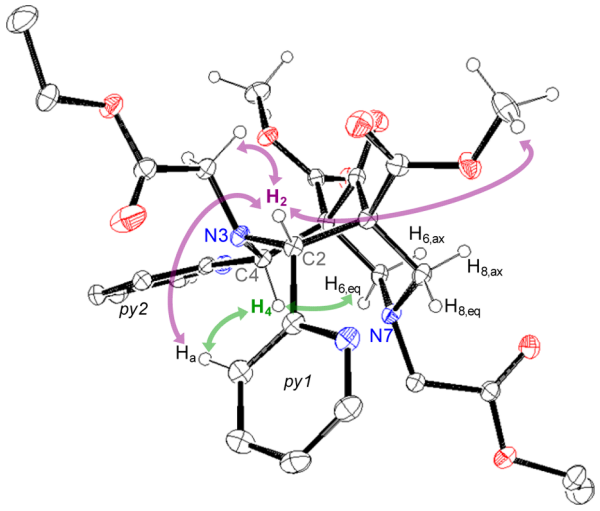

Figure 3. ORTEP drawing of ligand L_4 showing the main numbering scheme as well as through-space dipolar couplings involving H_2 (purple) and H_4 (green) in a $^1H-^1H$ NOESY experiment (400 MHz, $CDCl_3$). Thermal ellipsoids are drawn at the 30% probability level. H atoms are partially omitted for the sake of clarity.

crystallizes in a cc conformation with a *cis*-symmetrical arrangement of the pyridyl groups py1 and py2.[10] Other bispidone derivatives with bulky substituents in the N3 position, such as long alkyl chains (C_6, C_{12}, and C_{18}), have previously been synthesized by Sadler and co-workers, but they were isolated as oils. However, their NMR spectra are indicative of a cc conformation of the bicyclic ring together with a *cis* configuration of py1 and py2.[26] Taken together, all of these data appear to refute the initial hypothesis that the steric bulk of substituents in positions N3 and N7 is the determining factor for the stabilization of the boat conformation. To gain further insight into the driving force of the stereochemical behavior of diazacyclononanes, the solution structure of ligands L_1–L_4 has also been elucidated by solution NMR experiments, and the relative free energies of the *cis* and *trans* isomers have been investigated by using DFT calculations.

Structural Studies of L_1–L_4 in Solution. ^1H and ^{13}C spectroscopic studies on ligands L_1–L_4 were carried out in $CDCl_3$ and CD_3OD. The signals were completely assigned by using 2D-COSY spectra combined with $^1H-^1H$ NOESY experiments. The ^1H NMR spectra of L_1 (Figure S1, Supporting Information) and L_2 (Figure 4) display a single set of 13 and 11 signals, respectively, and point to the presence of a single isomer in solution with an effective C_S symmetry. The spectrum of L_1 is in agreement with literature data.[13] For both ligands, the signals due to protons H_2 and H_4 are observed as a singlet at δ = 4.69 ppm for L_1 and δ = 4.80 ppm for L_2 (see Scheme 2 for atom numbering). This is characteristic of bispidone derivatives that display a cc conformation with a *cis*-symmetrical arrangement of the pyridyl rings,[7,12,25] in line with the solid-state structures described above. The H_6 (or H_8) protons of ligand L_1 give rise to an AB spin system centered at δ = 2.95 ppm and with $^2J_{AB}$ = 12.4 Hz and $\Delta\nu_{AB}$ = 136 Hz, indicating a strong rigidity of the second cycle. Interestingly, no such rigidity was observed for ligand L_2 in $CDCl_3$, whereas an AB system ($^2J_{AB}$ = 12.2 Hz and $\Delta\nu_{AB}$ = 34 Hz) was observed in CD_3OD (Figure S2, Supporting Information). Moreover, through-space dipolar coupling was also observed between the protons H_a of the pyridine substituent and the low-field

dx.doi.org/10.1021/jo302248c | J. Org. Chem. 2012, 77, 11167–11176

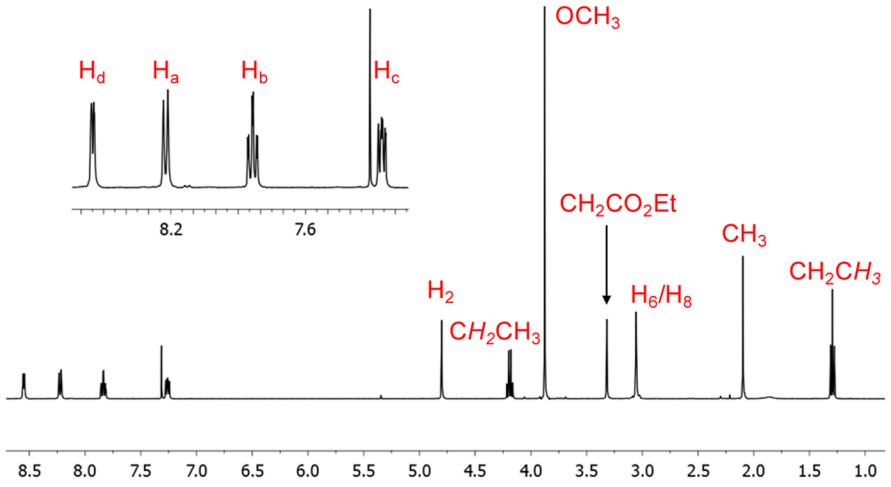

Figure 4. ^{1}H NMR spectrum of $\mathbf{L}_2$ (300 MHz, $CDCl_3$).

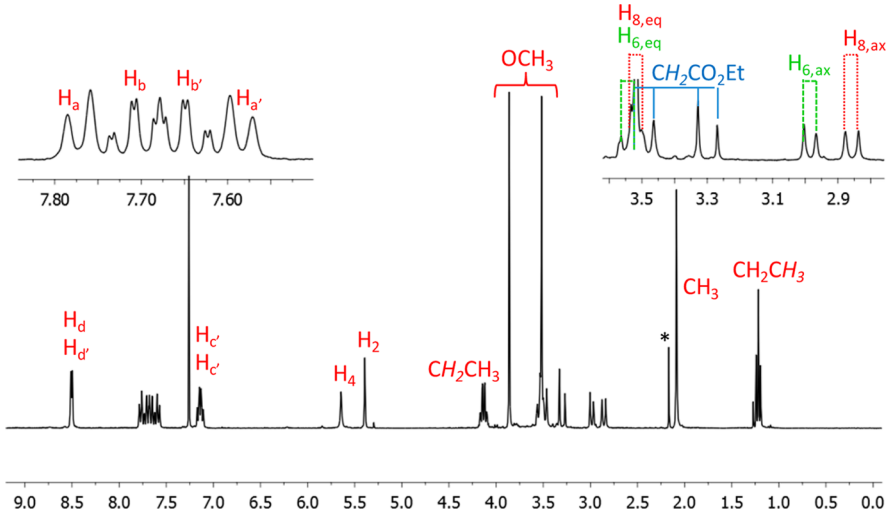

Figure 5. ^{1}H NMR spectrum of $\mathbf{L}_3$ (400 MHz, $CDCl_3$) with "∗" indicating residual acetone.

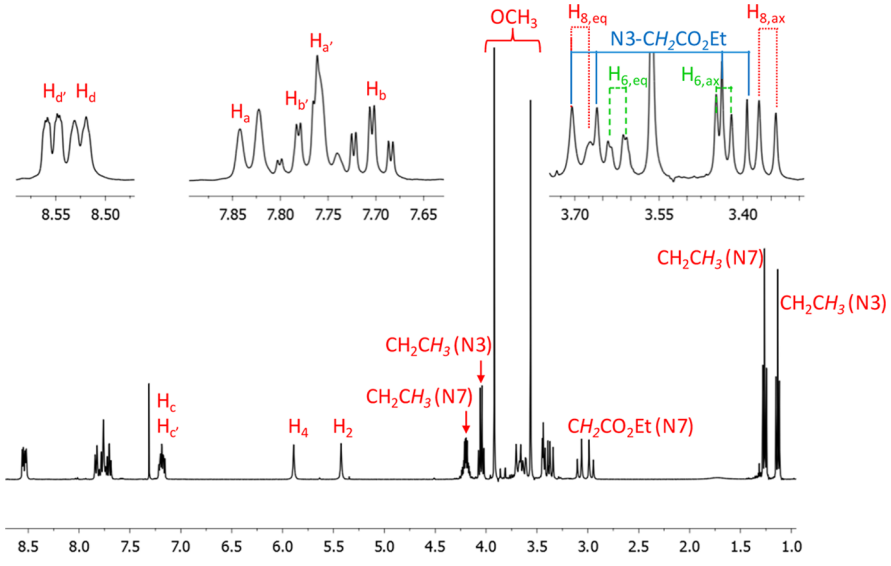

Figure 6. ^{1}H NMR spectrum of $\mathbf{L}_4$ (400 MHz, $CDCl_3$).

signal of the AB spin system arising from the protons H_{6eq}/H_{8eq}, pointing to their spatial proximity, as evidenced in the cc conformation observed in the solid-state structure (d = 2.8447(1) Å, Figure 1).

dx.doi.org/10.1021/jo302248c | J. Org. Chem. 2012, 77, 11167−11176

Ligands $\mathbf{L_3}$ and $\mathbf{L_4}$ give rise to more complex ^{1}H NMR spectra characterized by a lack of symmetry in comparison to the *cis* isomers (18 signals for $\mathbf{L_3}$ and 20 signals for $\mathbf{L_4}$, Figures 5 and 6). These patterns are characteristic of the presence of a single species in solution with C_1 symmetry. Interestingly, protons H_2 and H_4 appear as two singlets at δ = 5.39 ppm and δ = 5.64 ppm for $\mathbf{L_3}$, and δ = 5.37 ppm and δ = 5.84 ppm for $\mathbf{L_4}$. This pattern is indicative of a *trans* configuration of the pyridine substituents, in agreement with the solid-state structure of $\mathbf{L_4}$.[7] A 2D-COSY experiment combined with a ^{1}H−^{1}H NOESY experiment allowed the accurate assignment of all signals. The more shielded proton belongs to the hydrogen atom in the equatorial position (H_2). For both ligands, through-space dipolar coupling was observed between the proton H_2 and the CH_3 protons of the adjacent methyl ester, whereas no correlation was observed with the proton H_4 in the axial position (Figure 3; Figures S5 and S6, Supporting Information). Moreover, NOE effects are also clearly observed between H_2 and one of the CH_2 protons of the ethyl acetate substituent at N3 and between H_4 and the proton H_6 in the equatorial position. This is in agreement with distances observed in the solid-state structure of $\mathbf{L_4}$ ($d_{H_2-CH_2COOEt}$ = 2.307 Å, $d_{H_4-H_{6eq}}$ = 2.460 Å, Figure 3). As expected, no correlation has been observed between H_2 and the protons H_8 ($d_{H_2-H_8} \geq$ 3.504 Å, Figure 3) or between H_4 and the proton H_{6ax}. Finally, through-space dipolar coupling is also observed between H_4 and the pyridyl protons H_a and H_a', whereas the proton H_2 in the equatorial position only gives rise to NOE correlations with the proton H_a (Figure 3; Figures S4 and S5, Supporting Information). In all cases, these studies confirm that the introduction of an ethyl ester pendant arm in R_1 favors the boat conformation of the most substituted ring, which is in agreement with the solid-state structures of $\mathbf{L_3}$ and $\mathbf{L_4}$.

Molecular Geometries and Relative Energies of *Cis* and *Trans* Isomers. Geometry optimizations of compounds $\mathbf{L_1}$−$\mathbf{L_5}$ were performed by using DFT calculations (TPSSh functional). The $\mathbf{L_0}$ system, which contains methyl groups in positions N3 and N7, has also been modeled for comparison purposes. As expected, our calculations provided the *cis* and *trans* isomers as minimum energy conformations on the potential energy surface. The representative geometries of the *cis* and *trans* isomers of $\mathbf{L_1}$, $\mathbf{L_2}$, and $\mathbf{L_3}$ are shown in Figure 7.

According to our calculations, the diazabicyclononanone skeleton adopts preferentially a cc conformation in the *cis* isomers, whereas a bc conformation is observed for the *trans* isomers. In all cases, the substituents at positions N3 and N7 show an equatorial orientation. These molecular geometries are in agreement with the solid-state structures reported above. The relative free energies between the *cis* and the *trans* isomers of the $\mathbf{L_0}$−$\mathbf{L_5}$ systems are shown in Figure 8.

In the case of $\mathbf{L_0}$, calculations indicate that the *cis* isomer is more stable than the *trans* one by 6.42 kJ·mol^{-1}, which is in agreement with the solution structure of this compound determined by ^{1}H NMR spectroscopy.[29] The introduction of a 2-pyridylmethyl group in position N7 of the bispidone unit ($\mathbf{L_1}$) provokes a slight stabilization of the *cis* isomer (2.2 kJ·mol^{-1}), whereas the introduction of an ethylacetate group at N7 ($\mathbf{L_2}$) induces a considerable stabilization of the *trans* form. Indeed, the *trans* isomer remains less stable than the *cis* one, but only by −0.9 kJ·mol^{-1} in $\mathbf{L_2}$. The presence of either ethylacetate or 2-pyridylmethyl groups at position N3 stabilizes the *trans* isomer, which becomes the most stable form for $\mathbf{L_3}$−$\mathbf{L_5}$. The

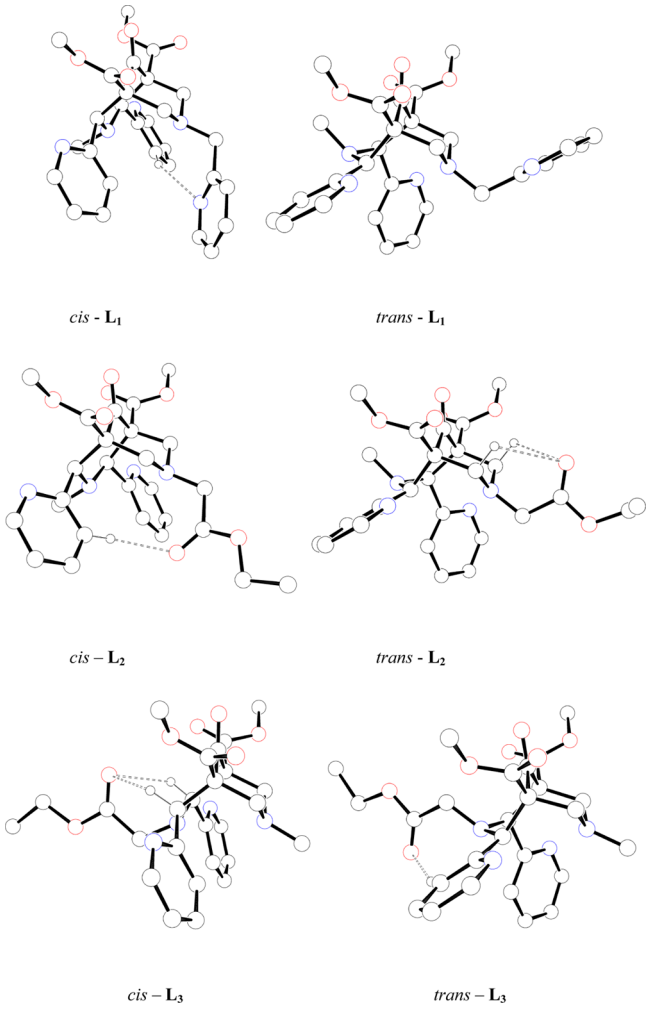

Figure 7. Molecular geometries of the *cis* and *trans* isomers of $\mathbf{L_1}$, $\mathbf{L_2}$, and $\mathbf{L_3}$ as optimized at the TPSSh/6-311G(d,p) level showing weak C−H···O hydrogen-bonding interactions. Hydrogen atoms, except those involved in hydrogen-bonding interactions, are omitted for simplicity.

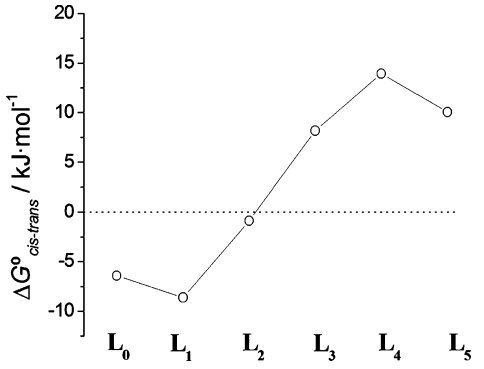

Figure 8. Relative free energies of the *cis* and *trans* isomers of $\mathbf{L_0}$−$\mathbf{L_5}$ calculated at the TPSSh/6-311G(d,p) level.

relative free energies shown in Figure 8 are in agreement with the experimental evidence, which shows that $\mathbf{L_0}$−$\mathbf{L_2}$ give the *cis* isomer as the most stable form in solution, whereas $\mathbf{L_3}$−$\mathbf{L_5}$ form either the *trans* isomer as a major species (as observed for $\mathbf{L_3}$ and $\mathbf{L_4}$) or, in the case of $\mathbf{L_5}$, a mixture of *cis* and *trans* isomers from which the *cis* isomer could be isolated in low yield (25%).[7]

dx.doi.org/10.1021/jo302248c | J. Org. Chem. 2012, 77, 11167−11176

These results suggest that the *trans* isomers of L_3−L_5 correspond to thermodynamically stable species rather than unusually stable kinetic products due to a particularly slow *trans*−*cis* isomerization process. The investigation of the *trans*−*cis* interconversion in L_2 and L_3 appears to confirm this hypothesis and is detailed below.

A detailed analysis of the optimized geometries of L_1−L_5 allows us to rationalize the different relative energies of *cis* and *trans* isomers in these closely related systems. Indeed, the relative stabilities of these isomers appear to be related to the presence of different weak hydrogen-bonding interactions involving the nitrogen atom of the pyridylmethyl or the carbonyl function of ethylacetate substituents as hydrogen-bonding acceptor groups, and C(sp^2)-H protons of the pyridyl rings at C2 and C4, or C(sp^3)-H protons at C2, C4, C6, and C8, as hydrogen-bonding donor groups. Representative examples of these hydrogen-bonding interactions are represented in Figure 7 and detailed in Table S1 (Supporting Information). Although the estimation of C−H···O bond energies is not straightforward, several studies concluded that they might fall within the range of 1.7−4.0 kJ·mol^{-1},[30] whereas C−H···N interactions are expected to be somewhat weaker.[31] Considering the relatively small energy differences shown in Figure 8, such interactions might have a sizable influence on the relative energies of *cis* and *trans* isomers in L_1−L_5.

The stabilization of the *cis* isomer of L_1 with respect to the situation observed for the parent system L_0 may be attributed to a weak hydrogen-bonding established between the pyridylmethyl substituent at position N7 and a C−H group of the pyridyl ring anchored at C2 (Figure 7; Table S1, Supporting Information), as observed in the solid-state structure (Figure 1). The hydrogen-bond parameters obtained after optimization are in good agreement with the distance observed in the crystalline structure of L_2 (vide supra). The introduction of a second pyridylmethyl group at N3 to give L_5 causes an important stabilization of the *trans* isomer. Inspection of the data reported in Table S1 (Supporting Information) shows that this can be attributed to the hydrogen-bonding interaction involving the nitrogen atom of the pyridylmethyl group at N3 and a C−H group of the pyridyl ring at C2. The relative stability of L_2, L_3, and L_4 appears to be the result of a subtle balance between the different hydrogen-bonding interactions that are established in the respective *cis* and *trans* isomers. These interactions include weak bifurcated hydrogen bonds involving CH groups at C6 and C8, or CH groups at C2 and C4, and the oxygen atom of the carbonyl function. Besides, C−H···O hydrogen bonds between the pyridyl ring at C2 and the carbonyl oxygen atom of the ester group are also formed. The introduction of ethylacetate groups at both N3 and N7 positions has a stabilizing effect on the *trans* isomer, but the effect is more pronounced if the substituent is attached in the N3 position. Taking these data as a whole, we conclude that the presence of hydrogen-bonding acceptor groups at N3 provokes an important stabilization of the *trans* isomer in these systems, due to the hydrogen-bonding interactions established with the pyridyl ring at C2.

***Trans*−*Cis* Isomerization Process in L_2 and L_3.** Previous semiempirical PM3 investigations on the kinetics of *trans*−*cis* isomerization in bicyclononanones showed that this process occurs through a retro-Mannich reaction by opening of the covalent bond between C1 and C2.[7] The retro-Mannich reaction requires the protonation of the keto carbonyl group to stabilize the ring-opened form as an enol. Theoretical calculations have been performed at the TPSSh/6-311G(d,p) level on models of the L_2 and L_3 systems in which the methylene carboxylic ethyl ester substituents have been replaced by methyl ester. Intermediates and transition states have been modeled and confirm that such a mechanism is indeed responsible for the *trans*−*cis* isomerization (Figure 9).

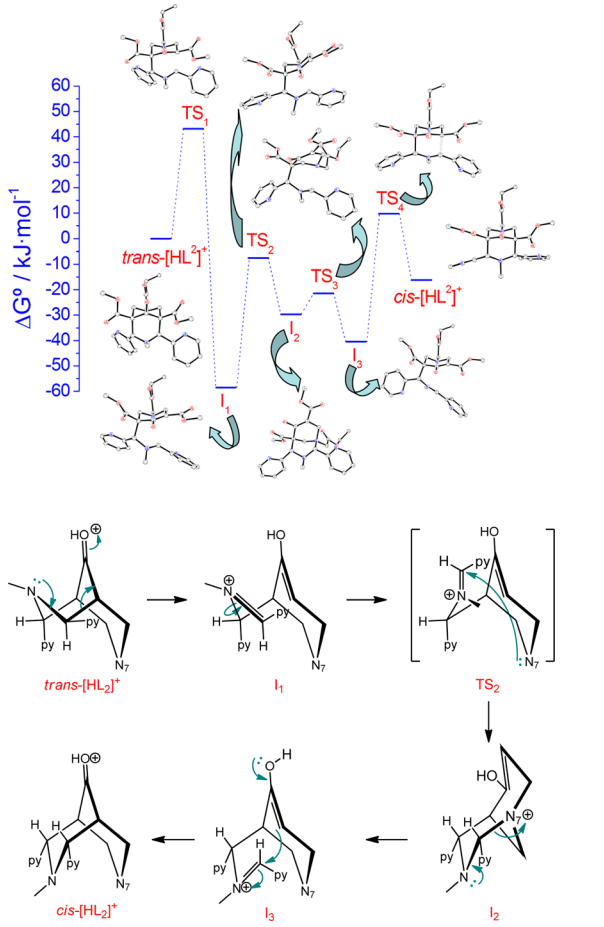

Figure 9. Diagram showing the energy minima, intermediates (I), and transition states (TS) obtained for the *trans*−*cis* isomerization of $[HL_2]^+$ at the TPSSh/6-311G(d,p) level (top) and the corresponding mechanism (bottom).

According to our calculations, the *trans* isomer of L_2 protonated on the keto carbonyl group can convert to enol I_1 through transition state TS_1. The C1−C2 distance, which amounts to 1.591 Å in *trans*-$[HL_2]^+$, increases to 2.034 Å in TS_1 and reaches 2.997 Å in I_1. Subsequent rotation of the C4−N3−C2−H dihedral brings the amine nitrogen N7 close to C2, resulting in the formation of intermediate I_2 through transition state TS_2. In I_2, the amine nitrogen atom at N7 forms a stable adduct by donating its lone pair to the carbon atom of the iminium function. This intermediate appears to be very stable (up to 58.5 kJ·mol^{-1} more stable than *trans*-$[HL_2]^+$ and 58.5 kJ·mol^{-1} more stable than *cis*-$[HL_2]^+$). However, it is worth mentioning that our DFT calculations have been performed in the gas phase on the protonated species, but this intermediate is expected to be considerably less stable in the presence of solvents with donor properties. The breaking of the N7−C2 bond leads to the open enol form I_3, which finally converts to the *cis*-$[HL_2]^+$ form through TS_4. Inspection of the energy diagram shown in Figure 9 shows that intermediates I_1, I_2, and

dx.doi.org/10.1021/jo302248c | J. Org. Chem. 2012, 77, 11167−11176

$\mathbf{I_3}$ have lower energies than the *cis*-$[\mathbf{HL_2}]^+$ form. However, one should bear in mind that this is only because these species are protonated and that the *trans*−*cis* interconversion process requires an additional step involving the deprotonation of the *cis*-$[\mathbf{HL_2}]^+$ form.

Considering the energy barriers calculated for the multistep processes responsible for the *trans*−*cis* isomerization, the opening of the bond between N7 and C2 is probably the rate-determining step of the interconversion process. In the case of $\mathbf{L_3}$, a similar interconversion pathway was obtained from our DFT calculations. The energy barriers involved in the *trans* ↔ *cis* isomerization process suggest that the formation of the *trans* isomer in $\mathbf{L_3}$ is related to the higher thermodynamic stability of this form with respect to the *cis* isomer.

CONCLUSIONS

Substituted diazabicyclo[3.3.1]nonane derivatives have interesting coordination properties, but their applications are, so far, limited by the small number of substituents that have been introduced in the N3 and N7 positions. Mostly, methyl, 2-pyridylmethyl, and 2-pyridylethyl derivatives have been synthesized. Larger residues were avoided because it was expected that they would induce conformational and configurational changes, such as chair/boat interconversion of the cycles with concomitant *cis*/*trans* isomerization of the aromatic moieties.

In this study, ethylacetate binding groups were introduced at N3 and/or N7 on a bispidone scaffold substituted by methylenecarboxylic ethyl ester groups. The incorporation of such strong binding groups is expected to increase the ligand affinity toward metal ions, such as Cu^{2+}. However, these structural changes were accompanied by a considerable stabilization of the *anti* isomer, which is detrimental to Cu^{2+} complexation. The relative energies of the *cis* and *trans* isomers have been modeled by density functional theory calculations. From this study, we can conclude that the stereochemistry of the bispidone skeleton is governed by thermodynamic rather than kinetic factors. Moreover, the relative stabilities of these isomers, which were, for a long time, correlated to steric hindrance only, appear to be also governed by the presence of weak H-bonding. The isomerization process has also been modeled by a four-step mechanism for which the ring-opening between C1 and C2 leading to the formation of an iminium transition state appears to be the rate-determining step.

This new understanding of the factors influencing bispidone stereochemistry will help us to select appropriate substituents to favor the *cis* isomer, thereby allowing the design of new bispidone ligands with enhanced affinity and selectivity for Cu^{2+}. Current efforts are focused in that direction.

EXPERIMENTAL SECTION

General Methods. Chemical shifts of ^{1}H and ^{13}C NMR spectra are reported in parts per million, with the residual protonated solvent as an internal reference.[32] IR spectra were recorded as solid samples, and only the most significant absorption bands are given in cm^{-1}.

X-ray Crystallography. Suitable crystals for X-ray diffraction were obtained for $\mathbf{L_1}$, $\mathbf{L_2}$, and $\mathbf{L_4}$. The crystals were placed in oil, and a single crystal was selected, mounted on a glass fiber, and placed in a low-temperature N_2 stream. Diffraction data for $\mathbf{L_2}$ and $\mathbf{L_4}$ were recorded on a diffractometer equipped with a cryosystem liquid N_2 device, using Mo Kα radiation (λ = 0.71073 Å). The crystal−detector distance was 36 mm. The cell parameters were determined from reflections taken from one set of 10 frames (1.0° steps in φ angle), each at a 20 s exposure (Denzo software).[33] The structures were solved by direct methods using the program SHELXS-97.[34] The refinement and all further calculations were carried out using SHELXL-97.[35] The H atoms were included in calculated positions and treated as riding atoms using SHELXL default parameters. The non-H atoms were refined anisotropically, using weighted full-matrix least-squares on F^2.

Diffraction data for $\mathbf{L_1}$ were recorded on a diffractometer equipped with a CCD camera and a graphite-monochromated Mo Kα radiation source (λ = 0.71073 Å) at 150(2) K. The Bruker SMART program was used to refine the values of the cell parameters. Data reduction and correction for absorption (SADABS) were carried out using the Bruker SAINT programs. The structure was solved by direct methods using the SIR97 program,[36] and then refined with full-matrix least-squares methods based on F^2 (SHELX-97)[37] with the aid of the WINGX program.[38] All non-hydrogen atoms were refined with anisotropic atomic displacement parameters. H atoms were finally included in their calculated positions.

Computational Methods. All calculations were performed employing DFT within the hybrid meta generalized gradient approximation (hybrid meta-GGA), with the TPSSh exchange-correlation functional,[39] and the Gaussian 09 package (revision A.02).[40] Full geometry optimizations of the $\mathbf{L_0}$−$\mathbf{L_5}$ systems were performed in vacuo by using the standard 6-311G(d,p) basis set. No symmetry constraints have been imposed during the optimizations. The default values for the integration grid ("fine") and the SCF energy convergence criteria (10^{-8}) were used. The stationary points found on the potential energy surfaces as a result of the geometry optimizations have been tested to represent energy minima rather than saddle points via frequency analysis. Relative free energies of the different minimum energy conformations obtained for each system include nonpotential-energy contributions (zero-point energies and thermal terms) obtained through frequency analysis. The interconversion between the *cis* and the *trans* forms of the $\mathbf{L_2}$ and $\mathbf{L_3}$ systems was investigated by using the synchronous transit-guided quasi-Newton method.[41,42] The nature of the saddle points and intermediates was characterized by frequency analysis. The free energy barriers include nonpotential energy contributions (that is, zero-point energies and thermal terms) obtained by frequency analysis.

Synthesis of the Ligands. Ligands $\mathbf{L_i}$ (i = 1−4) have been synthesized from the piperidinone precursors $\mathbf{P_1}$ and $\mathbf{P_2}$. Dimethyl-1-methyl-4-oxo-2,6-dipyridin-2-yl-3,5-dicarboxylate ($\mathbf{P_1}$)[26] and glycine ethyl ester[43] have been prepared according to literature procedures.

Dimethyl-1-carbethoxymethyl-4-oxo-2,6-dipyridin-2-yl-3,5-dicarboxylate ($\mathbf{P_2}$). 1,3-Acetonedicarboxylic acid dimethyl ester (0.84 mL, 5.81 mmol) was added dropwise to a solution of glycine ethyl ester (0.59 g, 5.81 mmol) and pyridine-2-aldehyde (1.11 mL, 11.62 mmol) in EtOH (6 mL) at 0 °C. After stirring at 0 °C for 30 min, crystallization of a yellow solid was observed. The solid was collected by filtration and recrystallized in hot EtOH to yield $\mathbf{P_2}$ as a white solid (1.62 g, 62%). mp 160−161 °C. ^{1}H NMR (300 MHz, $CDCl_3$, 25 °C): δ 1.20 (t, J = 7.1 Hz, 3H, OCH_2CH_3), 3.31 (AB system, δ_A = 3.24, δ_B = 3.37, J_{AB} = 17.0 Hz, 2H, CH_2COOEt), 3.61 (s, 3H, OCH_3), 3.71 (s, 3H, OCH_3), 4.09 (q, J = 7.1 Hz, 2H, OCH_2CH_3), 4.13 (d, J = 10.4 Hz, 1H, H_1), 4.64 (d, J = 10.4 Hz, 1H, H_2), 5.02 (s, 1H, H_4), 7.15 (m, 2H, py), 7.31 (d, J = 7.9 Hz, 1H, py), 7.57 (td, J_1 = 7.8 Hz, J_2 = 1.8 Hz, 1H, py), 7.74 (td, J_1 = 7.8 Hz, J_2 = 1.8 Hz, 1H, py), 8.02 (d, J = 7.8 Hz, 1H, py), 8.46 (dd, J_1 = 4.8 Hz, J_2 = 1.8 Hz, 1H, py), 8.54 (dd, J_1 = 4.8 Hz, J_2 = 1.8 Hz, 1H, py), 12.49 (s, 1H, OH). ^{13}C NMR (75 MHz, $CDCl_3$, 25 °C): δ 14.1, 45.2, 49.8, 51.7, 52.5, 52.6, 59.6, 60.6, 62.5, 98.0, 122.1, 122.6, 123.6, 123.7, 136.5, 148.4, 148.6, 157.7, 160.9, 166.7, 170.6, 171.7, 172.1. IR (cm^{-1}, ATR): ν 2959 (s, ν_{O-H}), 1735 (s, $\nu_{C=O\ ester}$), 1500−1700 (m, $\nu_{C=C\ Ar}$), 1248 (m, $\nu_{C-N\ Ar}$), 1206 (s, $\nu_{C\text{-}Oester}$). ES$^+$/MS: m/z = 456.18 ([M + H]$^+$, 100%). Anal. Calcd (mass %) for $C_{23}H_{25}N_3O_7$: C, 60.65; H, 5.53; N, 9.23. Found: C, 60.82; H, 5.62; N, 9.50.

Dimethyl-2,4-dipyridinyl-3-methyl-7-(pyridin-2-ylmethyl)-9-oxo-3,7-diazabicyclo[3.3.1]nonane-1,5-dicarboxylate ($\mathbf{L_1}$). Ligand $\mathbf{L_1}$ was obtained either from the peridinone $\mathbf{P_1}$ according to the procedure published by Börzel et al[13] or in a "one-pot" reaction in ethanol with a significantly higher yield. This modified procedure is reported below.

Pyridine-2-aldehyde (1.24 mL, 10.24 mmol) was added to a solution of 1,3-acetonedicarboxylic acid dimethyl ester (0.95 mL, 6.58 mmol) in EtOH (2 mL) at 0 °C . The solution was stirred at 0 °C for 15 min, and a solution of methylamine (40% in water) (0.56 mL, 6.38 mmol) in EtOH (1 mL) was added dropwise. The mixture was allowed to warm to room temperature, stirred for 30 min at 40 °C, and cooled down to room temperature to afford a beige precipitate. 2-Aminomethyl-pyridine (0.71 mL, 8.04 mmol) and a solution of formaldehyde (37% in water) (1.24 mL, 16.65 mmol) dissolved in EtOH (1 mL) were added to the resulting suspension. The mixture was heated for 1.5 h at 55 °C. After cooling to room temperature, white crystals were formed, which were collected by filtration, washed with cold EtOH, and dried under vacuum to yield $\mathbf{L_1}$ (1.45 g, 55%). mp 199−200 °C. ^{1}H NMR ($CDCl_3$, 300 MHz, 25 °C): δ 1.98 (s, 3H, N3-CH_3), 2.95 (AB system, δ_A = 3.18, δ_x = 2.72, J_{AB} = 12.4 Hz, 4H, H_8), 3.60 (s, 2H, N7-CH_2py3), 3.80 (s, 6H, OCH_3), 4.69 (s, 2H, H_2), 7.14 (dd, J_1 = 7.4 Hz, J_2 = 5.0 Hz, 2H, H_c), 7.27 (m, 1H, H_g), 7.37 (d, J = 7.7 Hz, 1H, H_e), 7.55 (td, J_1 = 7.7 Hz, J_2 = 1.9 Hz, 2H, H_b), 7.70 (td, J_1 = 7.6 Hz, J_2 = 1.8 Hz, 1H, H_f), 7.97 (d, J = 7.9 Hz, 2H, H_a), 8.45 (dd, J_1 = 4.9 Hz, J_2 = 1.7 Hz, 2H, H_d), 8.67 (dd, J_1 = 4.9 Hz, J_2 = 1.6 Hz, 1H, H_h).^{13}C NMR (75 MHz, $CDCl_3$, 25 °C): δ 43.1, 52.5, 58.8, 60.8, 63.6, 73.9, 122.4, 122.8, 123.8, 124.5, 136.3, 149.1, 149.6, 157.0, 158.5, 159.0, 168.5, 203.5. ES$^+$/MS: m/z = 516.3 ([M + H]$^+$, 100%). IR (cm^{-1}, ATR): ν 1736 (s, $\nu_{C=O\ ester}$), 1720 (s, $\nu_{C=O\ acetone}$), 1433−1590 (m, $\nu_{C=C\ Ar}$), 1278 (s, $\nu_{C-N\ Ar}$), 1164 (s, $\nu_{C-O\ ester}$).

Dimethyl-2,4-dipyridinyl-3-methyl-7-carbethoxymethyl-9-oxo-3,7-diazabicyclo[3.3.1]nonane-1,5-dicarboxylate ($\mathbf{L_2}$). Glycine ethyl ester (0.29 g, 2.86 mmol) and a 37% formaldehyde solution in water (0.58 mL, 7.80 mmol) were added to a suspension of piperidinone $\mathbf{P_1}$ (1.00 g, 2.60 mmol) in EtOH (6 mL) at room temperature. The reaction mixture was refluxed for 2 h, and the solution turned deep black. The solvent was removed under reduced pressure, and the remaining dark yellow solid was recrystallized from EtOH at 80 °C and dried under vacuum to obtain $\mathbf{L_2}$ as a white solid (0.81 g, 62%). mp 197−198 °C. ^{1}H NMR (400 MHz, $CDCl_3$, 25 °C): δ 1.29 (t, J = 7.2 Hz, 3H, OCH_2CH_3), 2.10 (s, 3H, N3-CH_3), 3.06 (s, 4H, H_8), 3.32 (s, 2H, N7-CH_2COOEt), 3.88 (s, 6H, OCH_3), 4.19 (q, J = 7.2 Hz, 2H, OCH_2CH_3), 4.80 (s, 2H, H_2), 7.26 (dd, J_1 = 7.6 Hz, J_2 = 4.9 Hz, 2H, H_c), 7.84 (td, J_1 = 7.7 Hz, J_2 = 1.8 Hz, 2H, H_b), 8.22 (d, J = 7.9 Hz, 2H, H_a), 8.55 (dd, J_1 = 4.9 Hz, J_2 = 1.6 Hz, 2H, H_d). ^{13}C NMR (75 MHz, $CDCl_3$, 25 °C): δ 14.2, 43.4, 52.5, 57.9, 60.6, 62.4, 73.7, 77.2, 123.0, 123.7, 136.5, 149.2, 158.8, 168.4, 169., 203.1. IR (cm^{-1}, ATR): ν 1729 (s, $\nu_{C=O\ ester}$), 1713 (s, $\nu_{C=O\ acetone}$), 1430−1588 (m, $\nu_{C=C\ Ar}$), 1252 (s, $\nu_{C-N\ Ar}$), 1157 (s, $\nu_{C-O\ ester}$). ES$^+$/MS: m/z = 511.21 ([M + H]$^+$, 100%). Anal. Calcd (mass %) for $C_{26}H_{30}N_4O_7$: C, 61.17; H, 5.92; N, 10.97. Found: C, 61.34; H, 5.98; N, 11.34. Single crystals of $\mathbf{L_2}$ suitable for X-ray diffraction analysis were obtained by slow evaporation of a 80 mM solution of $\mathbf{L_2}$ in MeOH.

Dimethyl-2,4-dipyridinyl-3-carbethoxymethyl-7-methyl-9-oxo-3,7-diazabicyclo[3.3.1]nonane-1,5-dicarboxylate ($\mathbf{L_3}$). Methylamine (0.06 mL, 0.52 mmol) and a 37% formaldehyde solution in water (0.01 mL, 1.29 mmol) were added to a suspension of piperidinone $\mathbf{P_2}$ (0.20 g, 0.43 mmol) in EtOH (2 mL). The mixture was refluxed for 3 h to give a red-brown solution. The solvent was evaporated under reduced pressure to give a brown oil that was refluxed in a minimum amount of EtOH for 15 min. After cooling to 4 °C, precipitation of a white solid occurred. The solid was recrystallized from EtOH at 80 °C and dried under vacuum to yield $\mathbf{L_3}$ as a white powder (0.18 g, 86%). mp 174−175 °C. ^{1}H NMR (400 MHz, $CDCl_3$, 25 °C): δ 1.21 (t, J = 7.2 Hz, 3H, OCH_2CH_3), 2.08 (s, 3H, N7-CH_3), 3.18 (AB system, δ_A = 3.92, δ_B = 2.44, J_{AB} = 11.8 Hz, 2H, H_8), 3.26 (AB system, δ_A = 3.54, δ_B = 2.98, J_{AB} = 10.7 Hz, 2H, H_6), 3.38 (AB system, δ_A = 3.48, δ_B = 3.30, J_{AB} = 17.8 Hz, 2H, N3-CH_2COOEt), 3.53 (s, 3H, OCH_3), 3.85 (s, 3H, OCH_3), 4.13 (q, J = 7.2 Hz, 2H, OCH_2CH_3), 5.39 (s, 1H, H_2), 5.64 (s, 1H, H_4), 7.14 (m, 2H, H_c + $H_{c'}$), 7.58 (d, J = 7.8 Hz, 1H, $H_{a'}$), 7.64 (td, J_1 = 7.8 Hz, J_2 = 1.8 Hz, 1H, $H_{b'}$), 7.70 (td, J_1 = 7.8 Hz, J_2 = 1.8 Hz, 1H, H_b), 7.76 (d, J = 7.8 Hz, 1H, H_a), 8.50 (m, 2H, H_d + $H_{d'}$). ^{13}C NMR (75 MHz, $CDCl_3$, 25 °C): δ 14.2, 43.8, 51.8, 52.0, 52.8, 60.6, 60.7, 62.5, 62.9, 65.5, 67.8, 68.5, 121.8 (2C), 122.0, 122.6, 136.3, 136.6, 148.5, 148.6, 158.7 (2C), 169.9, 170.5, 171.3, 204.8. IR (cm^{-1}, ATR): ν 1736 (s, $\nu_{C=O\ ester}$), 171 (s, $\nu_{C=O\ acetone}$), 1430−1600 (m, $\nu_{C=C\ Ar}$), 1252 (s, $\nu_{C-N\ Ar}$), 1168 (s, $\nu_{C-O\ ester}$). ES$^+$/MS: m/z = 511.22 ([M + H]$^+$, 100%). Anal. Calcd (mass %) for $C_{26}H_{30}N_4O_7$: C, 61.17; H, 5.92; N, 10.97. Found: C, 61.07; H, 5.96; N, 11.33.

Dimethyl-2,4-dipyridinyl-3,7-carbethoxymethyl-9-oxo-3,7-diazabicyclo[3.3.1]nonane-1,5-dicarboxylate ($\mathbf{L_4}$). Glycine ethyl ester (0.08 g, 0.74 mmol) and a 37% formaldehyde solution in water (0.14 mL, 1.83 mmol) were added to a suspension of piperidinone $\mathbf{P_2}$ (0.28 g, 0.61 mmol) in EtOH (10 mL) . The mixture was refluxed for 2 h, and the solution turned deep black. The solvent was removed under reduced pressure, and the remaining solid was recrystallized from EtOH at 80 °C and dried under vacuum to afford $\mathbf{L_4}$ as a white solid (0.31 g, 90%). mp 167−168 °C. ^{1}H NMR (400 MHz, $CDCl_3$, 25 °C): δ 1.08 (t, J = 7.2 Hz, 3H, N3-$CH_2CO_2CH_2CH_3$), 1.21 (t, J = 7.2 Hz, 3H, N7-$CH_2CO_2CH_2CH_3$), 2.97 (AB system, δ_A = 3.03, δ_B = 2.92, J_{AB} = 16.9 Hz, 2H, N7-CH_2CO_2Et), 3.51 (s, 3H, OCH_3), 3.47 (AB system, δ_A = 3.64, δ_B = 3.31, J_{AB} = 12.0 Hz, 2H, H_8), 3.48 (AB system, δ_A = 3.57, δ_B = 3.38, J_{AB} = 10.8 Hz, 2H, H_6), 3.50 (AB system, δ_A = 63, δ_B = 3.37, J_{AB} = 17.9 Hz, 2H, N3-CH_2CO_2Et), 3.87 (s, 3H, OCH_3), 3.99 (q, J = 7.1 Hz, 2H, N3-$CH_2CO_2CH_2CH_3$), 4.13 (qd, J_1 = 7.2 Hz, J_2 = 4.1 Hz, 2H, N7-$CH_2CO_2CH_2CH_3$), 5.37 (s, 1H, H_2), 5.84 (s, 1H, H_4), 7.14 (m, 2H, H_c + $H_{c'}$), 7.65 (td, J_1 = 7.6 Hz, J_2 = 1.9 Hz, 1H, H_b), 7.71 (m, 1H, $H_{a'}$), 7.73 (td, J_1 = 7.8 Hz, J_2 = 1.9 Hz, 1H, $H_{b'}$), 7.78 (d, J = 7.8 Hz, 1H, H_a), 8.50 (m, 2H, H_d + $H_{d'}$). ^{13}C NMR (75 MHz, $CDCl_3$, 25 °C): δ 14.0, 14.2, 51.7, 51.9, 52.9, 56.8, 57.8, 60.5, 60.7, 61.9, 62.9, 63.6, 67.2, 68.6, 121.3, 121.8, 121.8, 122.0, 136.4, 136.8, 148.4, 148.5, 158.3, 158.1, 169.7, 169.8, 170.7, 171.4, 205.4. IR (cm^{-1}, ATR): ν 1735 (s, $\nu_{C=O\ ester}$), 1706 (s, $\nu_{C=O\ acetone}$), 1433−1588 (m, $\nu_{C=C\ Ar}$), 1253 (m, $\nu_{C-N\ Ar}$), 1183 (s, $\nu_{C-O\ ester}$). ES$^+$/MS: m/z = 582.23 ([M$^\bullet$]$^+$, 100%). Anal. Calcd (mass %) for $C_{29}H_{34}N_4O_9$: C, 59.79; H, 5.88; N, 9.62. Found: C, 59.79; H, 5.93; N, 9.91. Single crystals of $\mathbf{L_4}$ suitable for X-ray diffraction analysis were obtained by slow evaporation of a 90 mM solution of $\mathbf{L_4}$ in MeOH.

■ ASSOCIATED CONTENT

Ⓢ Supporting Information

Additional spectroscopic data of $\mathbf{L_1}$, $\mathbf{L_2}$, $\mathbf{L_3}$, and $\mathbf{L_4}$; complete data and structure refinement, atomic coordinates, bond lengths and angles, and anisotropic displacement parameters for $\mathbf{L_1}$, $\mathbf{L_2}$, and $\mathbf{L_4}$ in CIF format; optimized molecular geometries of the *cis* and *trans* isomers of $\mathbf{L_0}$, $\mathbf{L_4}$, and $\mathbf{L_5}$; and optimized Cartesian coordinates obtained from DFT calculations. This material is available free of charge via the Internet at http://pubs.acs.org.

■ AUTHOR INFORMATION

Corresponding Author

*E-mail: aline.nonat@unistra.fr (A.M.N.), l.charbonn@unistra.fr (L.J.C.).

Notes

The authors declare no competing financial interest.

■ ACKNOWLEDGMENTS

This research was performed in the frame of the project "^{64}Cu radiolabeled nanomaterials for diagnostic and radiotherapy" (French ANR JCJC SIMI 7). This work was supported by the French Centre National de la Recherche Scientifique and the University of Strasbourg (UMR 7178). C.P.-I. gratefully acknowledged Centro de Supercomputación de Galicia (CESGA) for providing the computer facilities. The CDFIX of Rennes is also acknowledge.

■ REFERENCES

(1) Jeyraman, R.; Avila, S. *Chem. Rev.* **1981**, *81*, 149−174.

(2) Samhammer, A.; Holzgrabe, U. *Arch. Pharm. (Weinheim, Ger.)* **1989**, *322*, 551−555.
(3) Siener, T.; Cambareri, A.; Kuhl, U.; Englberger, W.; Haurand, M.; Kögel, B.; Holzgrabe, U. *J. Med. Chem.* **2000**, *43*, 3746−3751.
(4) Smith, G. S.; Thompson, M. D.; Berlin, K. D.; Holt, E. M.; Scherlag, B. J.; Petterson, E.; Lazarra, R. A. *Eur. J. Med. Chem.* **1990**, *25*, 1−8.
(5) Schön, U.; Antel, J.; Brückner, R.; Messinger, J. *J. Med. Chem.* **1998**, *41*, 318−331.
(6) Kuhl, U.; Englberger, W.; Haurand, M.; Holzgrabe, U. *Arch. Pharm. Pharm. Med. Chem.* **2000**, *333*, 226−230.
(7) Siener, T.; Holzgrabe, U.; Drosihn, S.; Brandt, W. *J. Chem. Soc., Perkin Trans. 2* **1999**, 1827−1834.
(8) Holzgrabe, U.; Brandt, W. *J. Med. Chem.* **2003**, *46*, 1383−1389.
(9) Fernande, M. J.; Huertas, R. M.; Galvez, E.; Orjales, A.; Berisa, A.; Labeaga, L.; Garcia, A. G.; Uceda, G.; ServerCarrio, J. *J. Mol. Struct.* **1995**, *2*−*3*, 203−213.
(10) Bleiholder, C.; Börzel, H.; Comba, P.; Ferrarri, R.; Heydt, M.; Kerscher, M.; Kuwata, S.; Laurenczy, G.; Lawrance, G. A.; Lienke, A.; Martin, B.; Merz, M.; Nuber, B.; Pritzkow, H. *Inorg. Chem.* **2005**, *44*, 8145−8155.
(11) Born, K.; Comba, P.; Ferrari, R.; Lawrance, G. A.; Wadepohl, H. *Inorg. Chem.* **2007**, *46*, 458−464.
(12) Comba, P.; Kuwata, S.; Linti, G.; Tarnai, M.; Wadepohl, H. *Eur. J. Inorg. Chem.* **2007**, 657−664.
(13) Börzel, H.; Comba, P.; Hagen, K. S.; Lampeka, Y. D.; Lienke, A.; Linti, G.; Merz, M.; Pritzkow, H.; Tsymbal, L. V. *Inorg. Chim. Acta* **2002**, *337*, 407−419.
(14) Comba, P.; Wadepohl, H.; Wiesner, S. *Eur. J. Inorg. Chem.* **2011**, 2610−2615.
(15) Comba, P.; Kuwata, S.; Tarnai, M.; Wadepohl, H. *Chem. Commun.* **2006**, 2074−2076.
(16) Comba, P.; Lopez de Laorden, C.; Pritzkow, H. *Helv. Chim. Acta* **2005**, *88*, 647−664.
(17) Benet-Buchholz, J.; Comba, P.; Llobet, A.; Roeser, S.; Vadivelu, P.; Wiesner, S. *Dalton Trans.* **2010**, *39*, 3315−3320.
(18) Juran, S.; Wather, M.; Stephan, H.; Bergmann, R.; Steinbach, J.; Kraus, W.; Emmerling, F.; Comba, P. *Bioconjugate Chem.* **2009**, *20*, 347−359.
(19) W Anderson, C. J. *Acc. Chem. Res.* **2009**, *42*, 832−841.
(20) Eckelman, W. C. *Drug Discovery Today* **2003**, *8*, 430−431.
(21) Knuuti, J.; Bengel, F. M. *Heart* **2008**, *94*, 360−367.
(22) Person, M.; Madsen, J.; Østergaard, S.; Jensen, M. M.; Jørgensen, J. T.; Juhl, K.; Lehmann, C.; Ploug, M.; Kjaer, A. *J. Nucl. Med.* **2012**, *53*, 138−145.
(23) Nielsen, C. H.; Kimura, R. H.; Withofs, N.; Tran, P. T.; Miao, Z.; Cochran, J. R.; Cheng, Z.; Felsher, D.; Kjær, A.; Willmann, J. K.; Gambhir, S. S. *Cancer Res.* **2010**, *70*, 9022−9030.
(24) Holzgrabe, U.; Erciyas, E. *Arch. Pharm.* **1992**, *325*, 657−663.
(25) Kuhl, U.; von Korff, M.; Baumann, K.; Burschka, C.; Holzgrabe, U. *J. Chem. Soc., Perkin Trans. 2* **2001**, 2037−2042.
(26) Barnes, N. A.; Brooker, A. T.; Godfrey, S. M.; Mallender, P. R.; Pritchard, R. G.; Sadler, M. *Eur. J. Org. Chem.* **2008**, 1019−1030.
(27) Comba, P.; Merz, M.; Pritzkow, H. *Eur. J. Inorg. Chem.* **2003**, 1711−1718.
(28) Comba, P.; Lopez de Laorden, C.; Pritzkow, H. *Helv. Chim. Acta* **2005**, *88*, 647−664.
(29) Haller, R.; Unholzer, H. *Arch. Pharm. (Weinheim, Ger.)* **1972**, *305*, 855−863.
(30) Desiraju, G. R.; Steiner, T. *The Weak Hydrogen Bond: In Structural Chemistry and Biology*; Oxford University Press: Oxford, U.K., 1999; Chapter 2.
(31) Bavafa, S.; Behjatmanesh-Ardakani, R.; Mashhadi, F. F. *J. Mol. Struct. (THEOCHEM)* **2010**, *960*, 15−21.
(32) Gottlieb, H. E.; Kottyar, K.; Nudelman, A. *J. Org. Chem.* **1997**, *82*, 7512−7515.
(33) *Kappa CCD Operation Manual*; Nonius B. V.: Delft, The Netherlands, 1997.
(34) Sheldrick, G. M. *Acta Crystallogr.* **1990**, *A46*, 467−473.
(35) Sheldrick, G. M. *SHELXL-97*; Universität Göttingen: Göttingen, Germany, 1999.
(36) Altomare, A.; Burla, M. C.; Camalli, M.; Cascarano, G.; Giacovazzo, C.; Guagliardi, A.; Moliterni, A. G. G.; Polidori, G.; Spagna, R. *J. Appl. Crystallogr.* **1999**, *32*, 115−119.
(37) Sheldrick, G. M. *Acta Crystallogr.* **2008**, *A64*, 112−122.
(38) Farrugia, L. J. *J. Appl. Crystallogr.* **1999**, *32*, 837−838.
(39) Tao, J. M.; Perdew, J. P.; Staroverov, V. N.; Scuseria, G. E. *Phys. Rev. Lett.* **2003**, *91*, 146401.
(40) Frisch, M. J.; Trucks, G. W.; Schlegel, H. B.; Scuseria, G. E.; Robb, M. A.; Cheeseman, J. R.; Scalmani, G.; Barone, V.; Mennucci, B.; Petersson, G. A.; Nakatsuji, H.; Caricato, M.; Li, X.; Hratchian, H. P.; Izmaylov, A. F.; Bloino, J.; Zheng, G.; Sonnenberg, J. L.; Hada, M.; Ehara, M.; Toyota, K.; Fukuda, R.; Hasegawa, J.; Ishida, M.; Nakajima, T.; Honda, Y.; Kitao, O.; Nakai, H.; Vreven, T.; Montgomery, J. A., Jr.; Peralta, J. E.; Ogliaro, F.; Bearpark, M.; Heyd, J. J.; Brothers, E.; Kudin, K. N.; Staroverov, V. N.; Kobayashi, R.; Normand, J.; Raghavachari, K.; Rendell, A.; Burant, J. C.; Iyengar, S. S.; Tomasi, J.; Cossi, M.; Rega, N.; Millam, N. J.; Klene, M.; Knox, J. E.; Cross, J. B.; Bakken, V.; Adamo, C.; Jaramillo, J.; Gomperts, R.; Stratmann, R. E.; Yazyev, O.; Austin, A. J.; Cammi, R.; Pomelli, C.; Ochterski, J. W.; Martin, R. L.; Morokuma, K.; Zakrzewski, V. G.; Voth, G. A.; Salvador, P.; Dannenberg, J. J.; Dapprich, S.; Daniels, A. D.; Farkas, Ö.; Foresman, J. B.; Ortiz, J. V.; Cioslowski, J.; Fox, D. J. *Gaussian 09*, revision A.01; Gaussian, Inc.: Wallingford, CT, 2009.
(41) Peng, C.; Ayala, P. Y.; Schlegel, H. B.; Frisch, M. J. *J. Comput. Chem.* **1996**, *17*, 49−56.
(42) Peng, C.; Schlegel, H. B. *Isr. J. Chem.* **1994**, *33*, 449−454.
(43) McKerrow, J. D.; Al-Rawi, J. M. A.; Brooks, P. *Synth. Commun.* **2010**, *40*, 1161−1179.